Superconductor Science and Technology

Nb/Au/$NbSe_2$ hybrid Josephson junctions

To cite this article before publication: Wanghao Tian *et al* 2021 *Supercond. Sci. Technol.* in press https://doi.org/10.1088/1361-6668/ac0f8f

Nb/Au/$NbSe_2$ hybrid Josephson junctions

Wanghao Tian,[1] Shixian Chen,[1] Zuyu Xu,[1] Dingding Li,[1] Hongmei Du,[1] Zihan Wei,[1] Kaixuan Wu,[1] Hancong Sun,[2] Sining Dong,[1] Yangyang Lv,[1] Yong-Lei Wang,[1] Dieter Koelle,[3] Reinhold Kleiner,[3] Huabing Wang,[1,2,*] and Peiheng Wu[1]

[1] *Research Institute of Superconductor Electronics, Nanjing University, Nanjing 210023, China*
[2] *Purple Mountain Laboratories, Nanjing University, Nanjing 211111, China*
[3] *Physikalisches Institut, Center for Quantum Science (CQ) and LISA$^+$, Universität Tübingen, D-72076 Tübingen, Germany*

(Dated: June 10, 2021)

We fabricated thin film Nb/Au/$NbSe_2$ hybrid Josephson junctions by a dry transfer technique with only a single lithography step in the process. A thin Au layer is deposited on Nb to prevent oxidation during the fabrication process. The superconducting van der Waals (vdW) material $NbSe_2$ is placed on top of the Nb/Au layer. Electrical transport properties are studied in detail and are compared to numerical simulations. The current-voltage characteristics we observe are typical for superconductor-normal metal-superconductor junctions and we do not observe an effect of a potential insulating barrier between $NbSe_2$ and Au. The modulation of the critical current in magnetic fields indicates an inhomogeneous distribution of supercurrent density, presumably caused by the roughness of the Nb/Au interface to $NbSe_2$. Nevertheless, we observe clear integer Shapiro steps, indicating a sinusoidal current phase relation of junctions. We do not see an impact of the anisotropic $s-$wave and the charge density wave in $NbSe_2$ on the Josephson effects. Our method presents a viable and simple way to fabricate hybrid Josephson junctions between superconducting films and two-dimensional (2D) vdW superconducting materials, which might offer a chance for widespread applications.

I. INTRODUCTION

Josephson junctions exhibiting unusual properties have always been a hot topic in condensed matter physics. Such unusual properties can arise from the barrier layer between the superconducting electrodes of the junction, or from the unusual properties of the superconductors. Well known examples are junctions with a (ferro)magnetic barrier[1–3], junctions between a conventional and a $d-$wave superconductor[4,5] or junctions involving a topological material[6,7]. Such junctions are not only interesting from the point of fundamental studies but also may lead to applications, e. g. in the context of quantum bits[6,8], digital electronics[9], field effect transistors[10] or microwave bolometers[11].

Recently, with the in-depth study of two-dimensional (2D) van der Waals (vdW) materials which are stable for even a thickness of only a few unit cells, contain only few atomic defects and have many unique properties[12], electronic devices based on heterostructures from such materials became popular[13,14]. In particular, a variety of novel structures for Josephson devices have emerged and broadened the research field. Here – in contrast to standard Josephson junctions where all layers are fabricated by thin film deposition – the 2D vdW materials are used as superconducting electrodes[15,16] or as barriers[17].

In this work, we fabricated Nb/Au/$NbSe_2$ hybrid Josephson junctions. 2H-$NbSe_2$, one kind of the 2D vdW transition metal dichalcogenides (TMDs) becoming superconducting below about 7.3 K, has versatile electronic and chemical properties, as well as many unique features such as an anisotropic superconducting $s-$wave gap[18], and the appearance of a charge density wave[19]. These features may make the material interesting for novel electronic devices.

Only few reports are available for Josephson junctions involving $NbSe_2$. All-$NbSe_2$ junctions and even SQUIDs are reported in Refs. 15 and 20. $NbSe_2$/Al junctions and SQUIDs have recently been reported in Ref. 21. A hybrid junction between 2D vdW crystals and superconducting thin films may be interesting for integrated circuits because of the flexibility of the film technology. Hybrid Josephson junctions might also be interesting for probing the physical properties of $NbSe_2$. In this respect, a Pb/Ag scanning tunneling microscope tip was used to form a Josephson junction to $NbSe_2$[22].

During the fabrication procedures, a key point is to properly handle the interfacial structure between the deposited films and the 2D vdW materials. The problem is two-fold: On the one hand, one needs to get clean surfaces of the 2D vdW materials with as little as possible degradation. On the other hand, the 2D vdW material and the thin films need to be close enough to get a metallic contact, while trying to avoid the damage of the 2D vdW material by the hits of atoms during the film depositions. While a dry-transfer of the vdW crystals to metallic structures to obtain good ohmic contacts is not uncommon[23], in the conventional Josephson junction processing, the interfaces are usually formed by depositing the thin films onto the 2D vdW materials. This may cause more defects in the 2D vdW materials during the deposition. Besides, the 2D vdW materials are exposed to air or are even exposed to chemicals over a long preparation time, making degradation likely.

In this paper, we propose a method to form Josephson junctions by transferring $NbSe_2$ directly onto the super-

conducting films, resulting in junctions between the films and the crystals. Transferring the crystal flakes onto the films, rather than depositing films subsequently, prevents the embedding of atoms into the 2D vdW material[24]. The surfaces of the cleaved crystal flakes are exposed to air only a short time and no chemical is used in the subsequent processing, which decreases the risk of degeneration of the crystals. A disadvantage of the method, however, is the roughness of the films and thus the interface to the 2D vdW materials.

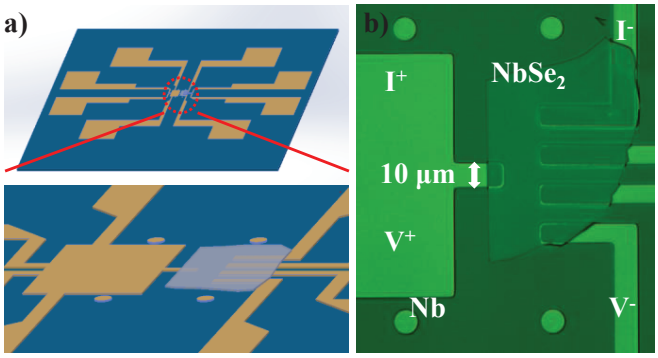

Figure 1. (a) Sketch of the junction and the Nb contacts (top graph). The lower graph is a zoom of the junction area. The yellow structures indicate the Nb electrodes, while the light blue structure indicates the $NbSe_2$ flake. (b) Optical microscope image of the junction area. The width of the junction is 10 μm. Connections of voltage and current leads are indicated.

We measure the electrical transport properties of the Nb/Au/$NbSe_2$ junctions for temperatures T down to 2.9 K, under microwave irradiation up to 30.1 GHz and with in-plane magnetic fields up to 6.3 mT. The current voltage characteristics (IVCs) are investigated and analyzed within numerical simulations based on an extension of the resistively and capacitively shunted junction model with an excess current (the so-called RCSJ+EX model[25]). We also discuss the magnetic field and temperature dependence of the critical current. The junctions in fact behave mostly conventional, and we do not see an impact of the $NbSe_2$ anisotropic $s-$wave and the charge density wave on the Josephson effects.

II. SAMPLE FABRICATION AND MEASUREMENT TECHNIQUES

In the beginning of the fabrication process, to obtain the electrodes contacting the $NbSe_2$ flakes, we pattern via direct laser writing photoresist covering a blank silicon substrate. Next, a 100 nm thick Nb film is deposited by magnetron sputtering and subsequently a layer of an about 2 nm thick Au film is deposited *in-situ* by electron-beam evaporation. The Au layer is intended to protect the surface of the Nb film from oxidation. After lift-off all Nb/Au electrodes are prepared. To obtain the $NbSe_2$ electrode, in a first step, about 1 μm thick flakes with an area of about 0.1 mm^2 are peeled off from a bulk $NbSe_2$ crystal with scotch tape. The flakes are subsequently placed onto a piece of polydimethylsiloxane (PDMS) and are further cleaved by a scotch tape under a microscope until a flat smooth surface is obtained. Then, the PDMS holding the $NbSe_2$ flake is pasted to the bottom of a glass slide mounted on a compact setup which consists of a semifixed microscope able to move along the z axis, a shelf below the microscope for holding a glass slide, and a platform below the shelf to place the substrate. Both the shelf and the platform can move along x, y, and z direction individually, while the platform can also be rotated manually. To transfer the $NbSe_2$ flake site-specifically onto the substrate, we first find the flake in the view field of the microscope then descend the microscope to view the substrate. We then descend the shelf slowly towards the substrate. When both the flake and the substrate can be seen in the view field of the microscope, one can align the shelf relative to the platform. Next, the substrate is heated to 70 °C for one minute to weaken the adhesion between the $NbSe_2$ flake and the PDMS. Subsequently, the glass slide is slowly lifted, leaving the $NbSe_2$ flakes on the substrate in contact with the Nb/Au electrode. Finally, the sample is slightly milled for 3 seconds with an Ar ion beam to remove the redundant Au film on the Nb electrodes, in order to avoid short-circuit currents through the Au film when measuring. Note that the Au film remains underneath the $NbSe_2$ flake, thus the junction formed is actually a Nb/Au/$NbSe_2$ junction.

In the whole process, only one lithography step is necessary to form the electrodes, and the $NbSe_2$ flakes are exposed to air for less than 3 minutes without any contacts to chemicals. Also the Nb/Au electrodes were in air for only 3 minutes after the lift-off process. Still, however, some contamination may have occurred during this time and may be in the future avoidable by preparing the sample in an *in-situ* glove box.

The geometry of our samples is shown in Fig. 1. Fig. 1(a) sketches the overall geometry in the top graph, and a zoom of the junction area is shown in the lower graph. The yellow structures indicate the Nb electrodes, while the light blue structure indicates the $NbSe_2$ flake. Fig. 1(b) is an optical image of the junction, with the voltage and current terminals indicated. A $10 \times 5\,\mu m^2$ rectangular junction is formed in the overlap region between Nb and $NbSe_2$, with a barrier consisting of a 2 nm Au layer and potentially a vdW contact to $NbSe_2$. The other four contacts on the right side of Fig. 1(b) serve as electrode terminals and also allow to perform a four-point measurement on the $NbSe_2$ flake. One may note that one side of the $NbSe_2$ flake is very even and straight. This is actually the surface of the original bulk $NbSe_2$ crystal. For our experiments we chose such straight sides in order to create a well-defined (rectangular) junction area.

We fabricated six junctions with different $NbSe_2$ thicknesses and junction areas. Data discussed in this paper are for the sample shown in Fig. 1(b), named junction

3. The other junctions had similar properties. In the supplement we display IVCs and inferred model parameters for these junctions, as well as selected microwave data for junction 2 and junction 4, and critical current vs. magnetic field patterns for junction 1 and junction 4. For junction 3 the $NbSe_2$ flake had a thickness of about 150 nm. The transition temperature T_c of this and other flakes used in our experiments is around 5 K, i. e. about 2 K less than the best values for $NbSe_2$ reported in the literature. The degradation presumably occurred during the 5 year storage time of the crystals in dry atmosphere.

We measured samples in a Gifford-McMahon refrigerator. The bias current was supplied by a homemade current source controlled by a computer while the voltage was filtered, amplified, and then measured. The microwave irradiation was generated by an Agilent N5183a MXG signal generator and transmitted through a semi-rigid cable mounted in the refrigerator with the core wire extruding at the end. The magnetic field was generated by a Helmholtz coil outside the refrigerator.

III. RESULTS

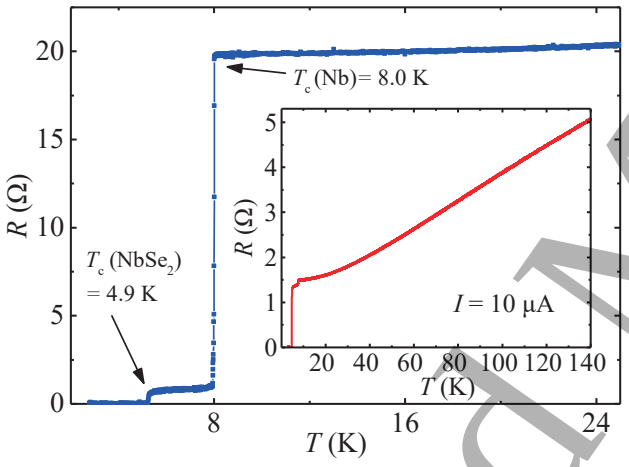

Figure 2. Temperature dependence of the sample resistance, measured across junction 3. The transition temperatures of Nb and $NbSe_2$ are indicated. The inset shows the resistance of the $NbSe_2$ flake for temperatures below 140 K. For both measurements the bias current is 10 μA.

Figure 2 shows the temperature dependence of the sample resistance, measured across junction 3 using the voltage and current terminals indicated in Fig. 1(b). At the critical temperature of Nb the resistance jumps from 20 Ω to about 0.9 Ω. The second jump occurs at the transition temperature of $NbSe_2$, at about 4.9 K. The inset of Fig. 2 shows the resistance of the $NbSe_2$ flake for temperatures below 140 K. The resistance decreases linearly down to about 40 K and starts to saturate at lower temperatures. There is a small jump at 7.5 K, and zero resistance is reached at 4.9 K. The small jump at 7.5 K is probably related to the onset of superconductivity in the Nb electrodes.

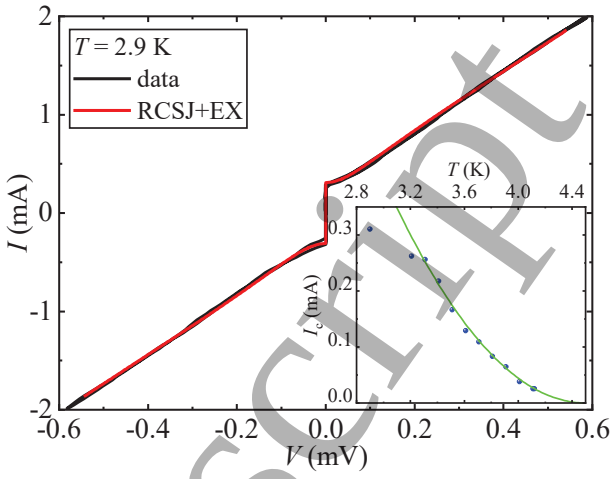

Figure 3. IVC of junction 3, measured at $T = 2.9$ K (black line). The red line is a fit based on the RCSJ+EX model with a Stewart-McCumber parameter $\beta_c = 0.1$, $i_{ex} = 0.65$ and $\alpha = 0.7$. The inset shows the temperature dependence of the junction critical current. The green line is the parabolic function $I_c \propto (1\text{-}T/4.5\,\mathrm{K})^2$.

The IVC measured at $T = 2.9$ K is shown by the black line in the main panel of Fig. 3. The junction critical current I_c is about 310 μA, and the critical current density amounts to 620 A/cm^2. For the full cycle of the bias current between ± 2 mA one finds a small hysteresis at negative current, however without a jump in voltage indicating capacitive or thermal effects. The hysteresis is likely to be caused by trapped flux in the $NbSe_2$ electrode. Apart from that, the IVC is single-valued and the voltage evolves smoothly in the resistive state. The overall IVC to a first glance reminds the IVC of an overdamped Josephson junction, as described in the resistively and capacitively shunted junction (RCSJ) model[26,27] for a McCumber parameter $\beta_c = 2\pi I_c R^2 C/\Phi_0$ well below 1. Here, $R \approx 0.32\,\Omega$ is the junction resistance, C the junction capacitance and Φ_0 the flux quantum. However, there is a substantial excess current $I_{ex} \approx 200\,\mu$A when extrapolating the linear part of the IVC back to zero voltage. The excess current can be caused by Andreev reflection processes in the junction.

Ideally, we either expect our junctions to be of the SNS or the SNIS type, where the normal conducting (N) layer corresponds to the Au layer covering the Nb electrode and the insulating (I) layer is due to a potential vdW gap between Au and $NbSe_2$. Other scenarios will be discussed at the end of section III. We do not see any tunneling-like features in the IVCs, thus the effect of an I layer seems to be negligible. This is also confirmed by the product of resistance times junction area, which is around $RA = 1.5\times10^{-7}\,\Omega\,\mathrm{cm}^2$, comparable to SNS junctions but four orders of magnitude lower than the RA product of

typical tunneling junctions.

For a quantitative description of the IVC we adopt the extended RCSJ model (RCSJ+EX model) introduced in Ref. 25. The model takes the effect of an excess current into account as an additional term in the RCSJ equations. In normalized form the RCSJ+EX model can be written as:

$$i + i_{\rm ac}\sin(f\tau) = \beta_{\rm c}\frac{{\rm d}^2\varphi}{{\rm d}\tau^2} + \frac{{\rm d}\varphi}{{\rm d}\tau} + \sin(\varphi) + i_{\rm ex}\tanh(\alpha\frac{{\rm d}\varphi}{{\rm d}\tau}), \quad (1)$$

φ is the Josephson phase difference. Currents are normalized to $I_{\rm c}$ and the time t is normalized as $\tau = 2\pi I_{\rm c}Rt/\Phi_0$. The dc voltage across the junction can be calculated by averaging ${\rm d}\varphi/{\rm d}\tau$. In the absence of the last term on the right hand side of equation 1 one returns to the standard RCSJ model. On the left hand side one finds the applied dc current i and an ac current $i_{\rm ac}\sin(f\tau)$, which will be used further below to analyze IVCs under microwave irradiation. In this term the frequency f is measured in units of the characteristic frequency $f_{\rm c} = I_{\rm c}R/\Phi_0$ (50 GHz in our case). The last term on the right hand side is related to the excess current, bringing in the two additional parameters $i_{\rm ex}$ and α. For large voltages the additional term produces a constant current $i_{\rm ex}$ while for low voltages the product $i_{\rm ex}\alpha$ constitutes an (voltage dependent) excess conductance. In Ref. 25 the additional parameters have been related to the parameters of the microscopic OTBK model[28].

In the RCSJ model $\beta_{\rm c}$ values below 0.3 or so have basically no impact on the shape of IVCs, compared to $\beta_{\rm c} = 0$. To get a very rough estimate of this parameter let us first assume a potential vdW gap between Au and $NbSe_2$ of order 1 nm. This results in a capacitance of about 0.4 pF. Using the values of $I_{\rm c}$ and R quoted above we crudely estimate $\beta_{\rm c} \approx 0.04$, which is rather indistinguishable from $\beta_{\rm c} = 0$. There may also be stray capacitances, thus for convenience we have set $\beta_{\rm c}$ to 0.1. For the fit shown by the red line in Fig. 3 we have used $i_{\rm ex} = 0.65$ and $\alpha = 0.7$. The resulting IVC matches the experimental data reasonably well. As shown in the inset of Fig. 3 the temperature dependence of the junction critical current (solid symbols) follows a parabolic temperature dependence above about 3.2 K, which is typical for SNS-type junctions. For the green line in the graph we have used the functionality $I_{\rm c} \propto (1\text{-}T/4.5\,{\rm K})^2$. The junction critical current goes to zero at about 4.5 K, i. e. somewhat below the $T_{\rm c}$ of $NbSe_2$.

Figure 4 displays by symbols the magnetic field dependence of the junction critical current, as obtained at $T = 2.9$ K. A voltage criterion at 5 μV was used to extract $I_{\rm c}$ from the IVCs. The direction of the applied magnetic field is in-plane and perpendicular to the 10 μm wide edge. Apparently, the experimental data strongly deviate from the Fraunhofer pattern, shown by the blue line, which would be obtained for a rectangular junction with homogeneous critical current density. Some deviations are likely to be caused by Abrikosov vortices in the $NbSe_2$ flake[29]. Although the (in-plane) lower critical field is presumably still somewhat higher than the maximum field of 9 mT we applied[30,31], we also have a relatively high transport current density in the $NbSe_2$ electrode which may lead to vortex entry at much smaller fields. Despite of such effects we must conclude that the Josephson critical current density of our junction is not very homogeneous. Using a London penetration depth of 110 nm for the Nb film[32] and a value of 140 nm for $NbSe_2$[33], plus the thicknesses of the Nb and $NbSe_2$ electrodes quoted above, we find an effective junction thickness[34] of about 115 nm, which would correspond to a modulation period of the Fraunhofer pattern of 1.8 mT. The modulation period we see in experiment is slightly shorter, an effect which can arise from flux focusing into the junction area. Further, from the critical current density, the London penetration depths and the thicknesses of the superconducting electrodes, we estimate a value of the Josephson penetration depth[34] of about 11 μm, i.e., we are in the short junction limit and self-field effects cannot account for the irregular critical current pattern. We also attempted to reconstruct the critical current density profile using the procedure of Ref. 35. However, we did not get a good agreement of the measured $I_{\rm c}$ vs. B patterns and the calculated ones resulting from the extracted critical current density profile. We are thus left with the qualitative statement of an inhomogeneous critical current density profile. Most likely, the inhomogeneity is caused by the roughness of the Nb/Au layer, which needs to be further improved, e. g. using the method described in Ref. 36.

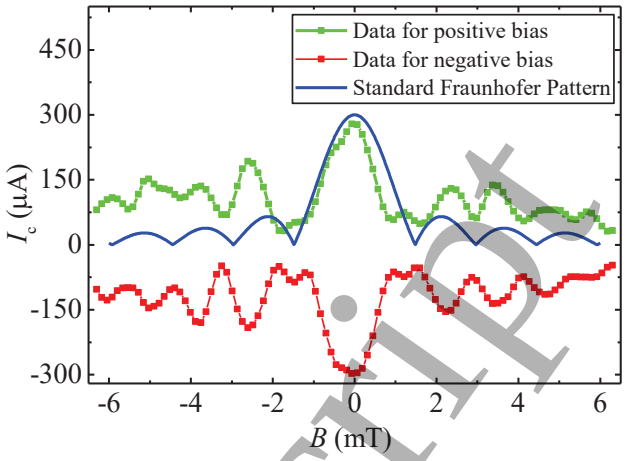

Figure 4. Magnetic field dependence of the junction critical current for positive and negative current bias (points) in comparison with the Fraunhofer dependence of the critical current expected for a homogeneous rectangular junction (blue line).

Let us finally discuss IVCs under 30.1 GHz microwave irradiation. The measurements once again probe spatially integrated properties of the junction and can give additional information whether the Josephson current-phase relation is sinusoidal or not. We use the Eq. 1 to model the data. Figure 5(a) shows by the solid symbols

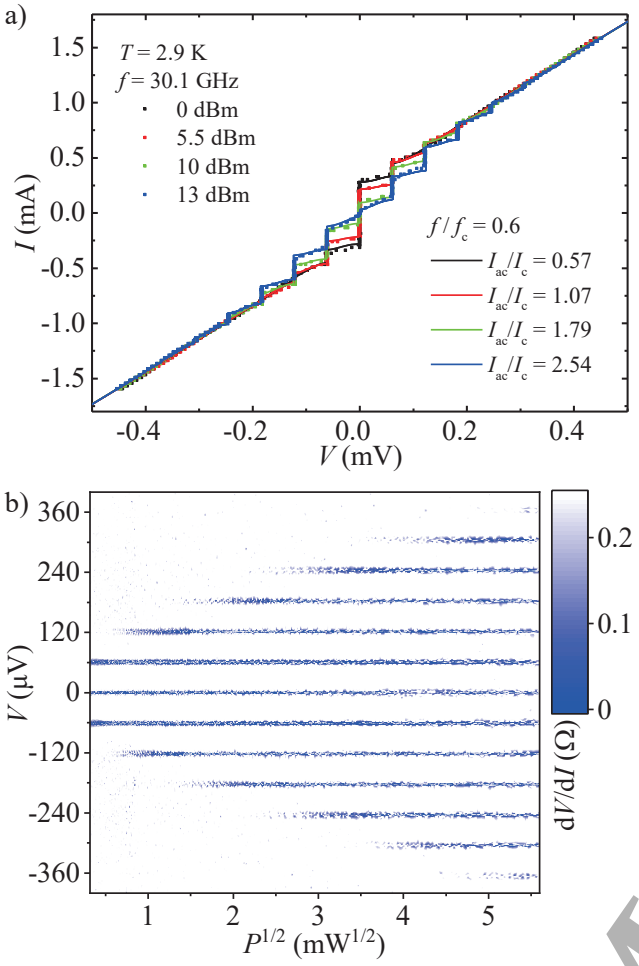

Figure 5. (a) IVCs of junction 3 under 30.1 GHz microwave irradiation for four different values of microwave power at $T = 2.9$ K. Lines are fits based on the RCSJ+EX model with the ac current normalized to I_c. (b) Color plot of the differential resistance dV/dI under 30.1 GHz microwave irradiation as a function of power amplitude $P^{1/2}$ and voltage V across the junction.

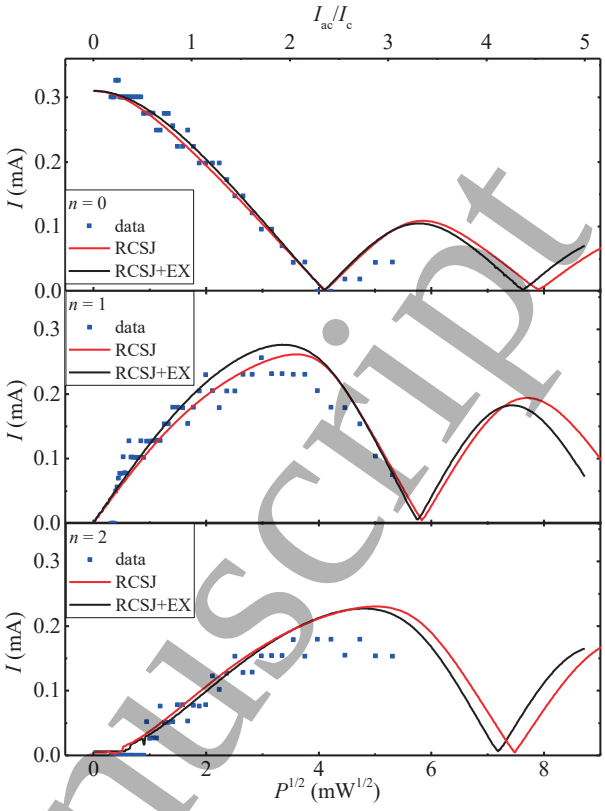

Figure 6. Heights of the zeroth, first and second Shapiro step (lower, middle and upper graph) in a 30.1 GHz microwave field as functions of microwave irradiation power. Blue squares are the experimental data while the black lines are the step heights, as calculated in the RCSJ+EX model. The normalized ac current is indicated on the top axis. Calibration with the experimental data is done so that the first minimum of step zero of the experimental and theoretical curves match. The red lines are based on the RCSJ model in the absence of an excess current. The ac currents are multiplied by 1.27 to match the first minimum of step zero with the RCSJ+EX curve.

the experimental IVCs of junction 3 for four different values of microwave power at $T = 2.9$ K. One observes Shapiro steps at (dimensioned) voltages $V = nf\Phi_0$, where n is an integer and $n = 0$ denotes the zero-voltage state. There is no evidence of subharmonic steps appearing at non-integer values of n. This can be seen more clearly in Fig. 5(b), where the junction differential resistance is shown by the color scale as a function of microwave amplitude $P^{1/2}$ and voltage V across the junction. The dark horizontal lines give the position of the Shapiro steps. When Eq. 1 is used to model the data, all parameters are fixed by the analysis of the IVC in the absence of microwave, except for one additional point relating the applied microwave amplitude to the ac current I_{ac}. This calibration is done by matching the microwave-induced first zero of the critical current (the $n = 0$ step), as shown in the top graph of Fig. 6. The simulated IVCs obtained using this calibration are shown by lines in Fig. 5(a), and Fig. 6 shows in the middle and bottom panel the dependence of the height of the first and second Shapiro step as a function of microwave amplitude. For completeness, we also show by red lines the step heights for $n = 0$, 1 and 2 calculated within the standard RCSJ model, i. e. for $i_{ex} = 0$. In this case the first zero of the $n = 0$ step occurs at a 21% lower value of the ac current as compared to the RCSJ+EX simulations, and we thus multiplied $i_{ac} = I_{ac}/I_c$ by 1.27 to facilitate the comparison. Apart from this scaling the step heights, obtained within the RCSJ and the RCSJ+EX model, are similar.

Thus, although all of our results indicate that an SNS-type Josephson junction with a sinusoidal current-phase relation has formed at the interface to the $NbSe_2$, let us also consider other possibilities. First we note that the $Nb/Au/NbSe_2$ interface must carry a supercurrent, because otherwise a serial resistance would be present also

at low bias current. The observed behavior might arise exclusively in the $NbSe_2$ crystal, in which case the interface must carry a supercurrent higher than the bias currents we applied. In principle, the Shapiro steps could arise from some synchronization of vortices moving in the $NbSe_2$ crystal. Such a synchronization was indeed observed[37]. However, the dependence of the Shapiro step heights on microwave power strongly differs from the dependence expected from RCSJ-type simulations, which is not the case for our junctions. Another possibility is that the interface carries a supercurrent but in the form of a few local weak links connecting Nb and $NbSe_2$. Such weak links may cause the excess current we observe. However, the weak links typically strongly suffer from Joule heating, producing hysteresis in the IVCs. In external microwave fields one observes Shapiro steps that appear on the return branch of the IVCs in the presence of hysteresis[38]. All this is not the case for the junction we observe and we thus conclude that we have fabricated genuine SNS-type junctions at the interface.

IV. SUMMARY

In summary we propose a simple method to fabricate $Nb/Au/NbSe_2$ Josephson junctions with only one lithography step in the fabrication process. Rather than depositing the metallic electrodes on top of $NbSe_2$ we place the $NbSe_2$ flake on the pre-patterned Nb/Au electrodes, avoiding damaging of the flake during thin film deposition and patterning. A drawback of our method is the roughness of the $Au/NbSe_2$ interface, which manifests itself in an inhomogeneous Josephson critical current density, as detected by the magnetic field dependence of the junction critical current. It seems possible that this roughness can be improved in the future. Electrically, the $Au/NbSe_2$ interface has a high transparency and our junctions behave very much like conventional SNS junctions, exhibiting some excess current in the current voltage characteristic and a parabolic temperature dependence of the junction critical current. In microwave fields we observe pronounced integer Shapiro steps but no sign of fractional steps, indicating a sinusoidal Josephson current-phase relation. The method proposed in this paper should be transferable also to other 2D vdW materials and thus may be interesting for (superconducting) electronics involving 2D vdW materials in contact to metallic electrodes.

ACKNOWLEDGMENTS

We gratefully acknowledge financial support by the National Natural Science Foundation of China (Grant Nos. 61727805, 11961141002, 61521001, 61771235), the National Key R&D Program of China (Grant No. 2018YFA0209002), Jiangsu Key Laboratory of Advanced Techniques for Manipulating Electromagnetic Waves, and the EU-FP6-COST Action CA16218.

* Emails: hbwang@nju.edu.cn, kleiner@uni-tuebingen.de

[1] L. B. Bulaevskii, V. V. Kuzii, and A. A. Sobyanin, "Superconducting system with weak coupling to the current in the ground state," JETP Lett. **25**, 290 (1977).
[2] A. I. Buzdin and M. Yu. Kupriyanov, "Josephson junction with a ferromagnetic layer," JETP Lett. **53**, 321 (1991).
[3] V. V. Ryazanov, V. A. Oboznov, A. Yu. Rusanov, A. V. Veretennikov, A. A. Golubov, and J. Aarts, "Coupling of two superconductors through a ferromagnet: Evidence for a π junction," Phys. Rev. Lett. **86**, 2427 (2001).
[4] J. H. Xu, J. L. Shen, J. H. Miller, and C. S. Ting, "Superconducting pairing symmetry and Josephson tunneling," Phys. Rev. Lett. **73**, 2492 (1994).
[5] C. C. Tsuei and J. R. Kirtley, "Pairing symmetry in cuprate superconductors," Rev. Mod. Phys. **72**, 969 (2000).
[6] Leonid P. Rokhinson, Xinyu Liu, and Jacek K. Furdyna, "The fractional a.c. Josephson effect in a semiconductor-superconductor nanowire as a signature of Majorana particles," Nat. Phys. **8**, 795 (2012).
[7] J. Wiedenmann, E. Bocquillon, R. S. Deacon, S. Hartinger, O. Herrmann, T. M. Klapwijk, L. Maier, C. Ames, C. Brüne, C. Gould, A. Oiwa, K. Ishibashi, S. Tarucha, H. Buhmann, and L. W. Molenkamp, "4π-periodic Josephson supercurrent in HgTe-based topological Josephson junctions," Nat. Comm. **7**, 10303 (2016).
[8] A. K. Feofanov, V. A. Oboznov, V. V. Bolginov, J. Lisenfeld, S. Poletto, V. V. Ryazanov, A. N. Rossolenko, M. Khabipov, D. Balashov, A. B. Zorin, P. N. Dmitriev, V. P. Koshelets, and A. V. Ustinov, "Implementation of superconductor/ferromagnet/superconductor π-shifters in superconducting digital and quantum circuits," Nature Physics **6**, 593 (2010).
[9] T. Ortlepp, Ariando, O. Mielke, C. J. M. Verwijs, K. F. K. Foo, H. Rogalla, F. H. Uhlmann, and H. Hilgenkamp, "Flip-flopping fractional flux quanta," Science **312**, 1495 (2006).
[10] Pablo Jarillo-Herrero, Jorden A. Van Dam, and Leo P. Kouwenhoven, "Quantum supercurrent transistors in carbon nanotubes," Nature **439**, 953 (2006).
[11] Gil-Ho Lee, Dmitri K. Efetov, Woochan Jung, Leonardo Ranzani, Evan D. Walsh, Thomas A. Ohki, Takashi Taniguchi, Kenji Watanabe, Philip Kim, Dirk Englund, and Kin Chung Fong, "Graphene-based Josephson junction microwave bolometer," Nature **586**, 42 (2020).
[12] Sheneve Z. Butler, Shawna M. Hollen, Linyou Cao, Yi Cui, Jay A. Gupta, Humberto R. Gutiérrez, Tony F. Heinz, Seung Sae Hong, Jiaxing Huang, Ariel F. Ismach, Ezekiel Johnston-Halperin, Masaru Kuno, Vladimir V. Plashnitsa, Richard D. Robinson, Rodney S. Ruoff, Sayeef Salahuddin, Jie Shan, Li Shi, Michael G. Spencer, Mauricio Terrones, Wolfgang Windl, and Joshua E. Goldberger, "Progress,

challenges, and opportunities in two-dimensional materials beyond graphene," ACS Nano **7**, 2898 (2013).

[13] A. K. Geim and I. V. Grigorieva, "Van der Waals heterostructures," Nature **499**, 419 (2013).

[14] Deep Jariwala, Tobin J. Marks, and Mark C. Hersam, "Mixed-dimensional van der Waals heterostructures," Nat. Mater. **16**, 170 (2017).

[15] Naoto Yabuki, Rai Moriya, Miho Arai, Yohta Sata, Sei Morikawa, Satoru Masubuchi, and Tomoki Machida, "Supercurrent in van der Waals Josephson junction," Nat. Comm. **7**, 10616 (2016).

[16] Tom Dvir, Ayelet Zalic, Eirik Holm Fyhn, Morten Amundsen, Takashi Taniguchi, Kenji Watanabe, Jacob Linder, and Hadar Steinberg, "Planar graphene-$NbSe_2$ Josephson junctions in a parallel magnetic field," Phys. Rev. B **103**, 115401 (2021).

[17] Gil-Ho Lee, Sol Kim, Seung-Hoon Jhi, and Hu-Jong Lee, "Ultimately short ballistic vertical graphene Josephson junctions," Nat. Comm. **6**, 6181 (2015).

[18] T. Yokoya, "Fermi surface sheet-dependent superconductivity in 2H-$NbSe_2$," Science **294**, 2518 (2001).

[19] J. C. Tsang, J. E. Smith, and M. W. Shafer, "Raman Spectroscopy of Soft Modes at the Charge-Density-Wave Phase Transition in 2H-$NbSe_2$," Phys. Rev. Lett. **37**, 1407 (1976).

[20] L. S. Farrar, A.Nevill, Z. J. Lim, G. Balakrishnan, S. Dale, and S. J. Bending, "Superconducting quantum interference in twisted van der Waals heterostructures," ArXiv:2101.04551 (2021).

[21] Michael R. Sinko, Sergio C. de la Barrera, Olivia Lanes, Kenji Watanabe, Takashi Taniguchi, Susheng Tan, David Pekker, Michael Hatridge, and Benjamin M. Hunt, "Superconducting contact and quantum interference between two-dimensional van der Waals and three-dimensional conventional superconductors," Phys. Rev. Materials **5**, 014001 (2021).

[22] O. Naaman, R. C. Dynes, and E. Bucher, "Josephson effect in Pb/I/$NbSe_2$ scanning tunneling microscope junctions," International Journal of Modern Physics B **17**, 3569 (2003).

[23] Masahiko Yokoi, Satoshi Fujiwara, Tomoya Kawamura, Tomonori Arakawa, Kazushi Aoyama, Hiroshi Fukuyama, Kensuke Kobayashi, and Yasuhiro Niimi, "Negative resistance state in superconducting $NbSe_2$ induced by surface acoustic waves," Sci. Adv. **6**, eaba1377 (2020).

[24] Momoko Onodera, Satoru Masubuchi, Rai Moriya, and Tomoki Machida, "Assembly of van der Waals heterostructures: exfoliation, searching, and stacking of 2D materials," Japanese Journal of Applied Physics **59**, 010101 (2020).

[25] Peter Baars, Andreas Richter, and Ulrich Merkt, "Temperature and power dependence of Shapiro and Fiske step widths in Nb/InAs/Nb Josephson junctions," Phys. Rev. B **67**, 224501 (2003).

[26] W. C. Stewart, "Current-Voltage characteristics of Josephson junctions," Appl. Phys. Lett. **12**, 277 (1968).

[27] D. E. McCumber, "Effect of ac Impedance on dc Voltage-Current Characteristics of Superconductor Weak Link Junctions," J. Appl. Phys. **39**, 3113 (1968).

[28] M. Octavio, M. Tinkham, G. E. Blonder, and T. M. Klapwijk, "Subharmonic energy-gap structure in superconducting constrictions," Phys. Rev. B **27**, 6739 (1983).

[29] I. Fridman, C. Kloc, C. Petrovic, and J. Y. T. Wei, "Lateral imaging of the superconducting vortex lattice using Doppler-modulated scanning tunneling microscopy," Appl. Phys. Lett. **99**, 192505 (2011).

[30] E. Boaknin, M. A. Tanatar, J. Paglione, D. Hawthorn, F. Ronning, R. W. Hill, M. Sutherland, L. Taillefer, J. Sonier, S. M. Hayden, and J. W. Brill, "Heat Conduction in the Vortex State of $NbSe_2$: Evidence for Multiband Superconductivity," Phys. Rev. Lett. **90**, 117003 (2003).

[31] P. D. Trey, S. Gygax, and J. P. Jan, "Anisotropy of the Ginzburg-Landau parameter κ in $NbSe_2$," J. Low Temp. Phys. **11**, 421 (1973).

[32] A. I. Gubin, K. S. Il'in, S. A. Vitusevich, M. Siegel, and N. Klein, "Dependence of magnetic penetration depth on the thickness of superconducting Nb thin films," Phys. Rev. B **72**, 064503 (2005).

[33] J. D. Fletcher, A. Carrington, P. Diener, P. Rodière, J. P. Brison, R. Prozorov, T. Olheiser, and R. W. Giannetta, "Penetration depth study of superconducting gap structure of $2H-NbSe_2$," Phys. Rev. Lett. **98**, 057003 (2007).

[34] M. Weihnacht, "Influence of film thickness on d. c. Josephson current," Phys. Stat. Sol. **32**, K169 (1969).

[35] R. C. Dynes and T. A. Fulton, "Supercurrent density distribution in Josephson junctions," Phys. Rev. B **3**, 3015 (1971).

[36] Yu Wu, Liliang Ying, Guanqun Li, Xue Zhang, Wei Peng, Jie Ren, and Zhen Wang, "Film stress influence on Nb/Al-AlO_x/Nb Josephson junctions," IEEE Transactions on Applied Superconductivity **29**, 1 (2019).

[37] S. Tran, J. Sell, and J. R. Williams, "Dynamical Josephson effects in $NbSe_2$," Phys. Rev. Res. **2**, 043204 (2020).

[38] Connor D. Shelly, Patrick See, Ivan Rungger, and Jonathan M. Williams, "Existence of Shapiro Steps in the Dissipative Regime in Superconducting Weak Links," Phys. Rev. Applied **13**, 024070 (2020).